Supplementary Information: Flexible and tunable silicon photonic circuits on plastic substrates

Yu Chen[1], Huan Li[1], and Mo Li[11]

[1]*Department of Electrical and Computer Engineering, University of Minnesota, Minneapolis, MN 55455, USA*

1. Mechanical tuning of flexible photonic devices

In the experimental demonstration that the Mach-Zehnder interferometer devices (MZI) on the PDMS substrate can be mechanically tuned, it was observed that the interference fringes shift toward shorter wavelengths (i.e. blue shift) when the substrate is compressed. In the following we describe a theoretical model on the mechanical tunability of flexible photonic devices on plastic substrates, based on the experimental results and theories of flexible electronics[1-5].

a) Buckling of silicon waveguide on a flexible substrate

Subject to compression beyond the critical value of strain, a composite structure consisting of a thin film of stiff material (e.g. silicon) on a substrate of compliant material (e.g. PDMS) can form periodic buckling in a sinusoidal wave pattern while the film remains bonded to the substrate, as shown in Figure S1. Mechanics models have been developed to explain ripples and wrinkles in such a system in the context of flexible and stretchable electronic devices. With small displacement approximation, the periodic wave out-of-plane displacement w and its amplitude A of buckling when strain ε_a (negative if

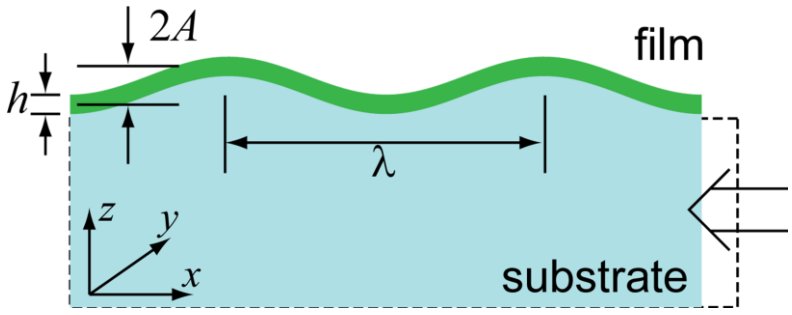

Figure S1 Periodically buckled film on a compliant substrate when a compressive strain is applied.

compressive) is applied are given by[3,4]:

$$w = A\cos(\frac{2\pi}{\lambda}x) \quad (1)$$

$$A = h\sqrt{-\varepsilon_a / \varepsilon_c - 1} / (1+\tfrac{27}{32}\varepsilon_a) \quad (2)$$

Here, it is assumed that the structure is relaxed initially (i.e. zero initial strain). λ is the period of the ripple and ε_c is the critical value of strain above which the film buckles. They are given by the following equations derived from the elastic plate theory:

$$\varepsilon_c = \frac{1}{4}(\frac{3\bar{E}_s}{\bar{E}_f})^{2/3} \quad (3)$$

$$\lambda = 2\pi h(\frac{\bar{E}_f}{3\bar{E}_s})^{1/3}\frac{1+\varepsilon_a}{(1+27/32\,\varepsilon_a)^{1/3}} \quad (4)$$

where h is the thickness of the film, $\bar{E}_f = E_f/(1-\upsilon_f^2)$ and $\bar{E}_s = E_s/(1-\upsilon_s^2)$, E_f and E_s, υ_f and υ_s are the plain-strain modulus, Young's modulus and Poisson ratio of the film and the substrate materials, respectively. In the Si/PDMS system, using the mechanical properties listed in Table 1, the critical strain ε_c is evaluated to be 0.03%. This value is significantly smaller than the minimum compressive strain that can be reliably applied in our experiment. So the waveguides are always in the buckled mode during the tuning experiment.

Table 1 Mechanical properties of silicon and PDMS

	Young's Modulus E	**Poisson ratio** υ	**Plain-strain Modulus** $\bar{E}$
Si	130 GPa	0.27	140 GPa
PDMS	1.8 MPa	0.48	2.3 MPa

When the buckling amplitude A is small compared with the wavelength λ and sheer stress is neglected, the strain field can be approximated to be uniform in the film with an average value given by[3]:

$$\varepsilon_{xx} = (\pi A/\lambda)^2,\ \ \varepsilon_{yz} = \varepsilon_{xy} = 0 \quad (5)$$

In our experiment, the maximal compression that is applied to the MZI device with a substrate width of 1cm is 300 μm. Thus the corresponding maximal applied compressive

strain is -3%. Using equations (2) and (4), the buckling amplitude A is calculated to be 2.1 μm, which is much smaller than the ripple wavelength λ of 37.3 μm. Thus the above small deflection approximation and the consequent assumption of uniform strain field are valid in our situation. Using equations (2), (4) and (5), the uniform normal strain in the film can be expressed in term of the applied strain as:

$$\varepsilon_{xx} = \frac{(-\varepsilon_a / \varepsilon_c - 1)}{4(\overline{E_f} / 3\overline{E_s})^{2/3}(1 + 27/32\,\varepsilon_a)^{4/3}(1+\varepsilon_a)^2} \tag{6}$$

b) Photo-elastic effect in strained silicon waveguide

We next considered the photo-elastic effect in a silicon waveguide that is buckled when a uniaxial strain is applied to the compliant substrate. Ignoring in-plane shear stress, the strain tensor in this buckled silicon waveguide could be written as:

$$\varepsilon = \begin{pmatrix} \varepsilon_{xx} \\ \varepsilon_{yy} \\ \varepsilon_{zz} \\ \varepsilon_{yz} \\ \varepsilon_{zx} \\ \varepsilon_{xy} \end{pmatrix} = \begin{pmatrix} \varepsilon_{xx} \\ -\upsilon\varepsilon_{xx} \\ -\upsilon\varepsilon_{xx} \\ 0 \\ \varepsilon_{zx} \\ 0 \end{pmatrix} \tag{7}$$

The strain field induces photo-elastic effect and changes in the refractive index matrix in silicon as described by[6]:

$$\Delta(\frac{1}{n^2})_i = \sum_{j=1}^{6} p_{ij}\varepsilon_j \tag{8}$$

where p_{ij} are the elements of the elasto-optic coefficient matrix. Silicon has a cubic crystal structure so its elasto-optic coefficient matrix reduces to:

$$p_{ij} = \begin{pmatrix} p_{11} & p_{12} & p_{12} & 0 & 0 & 0 \\ p_{12} & p_{11} & p_{12} & 0 & 0 & 0 \\ p_{12} & p_{12} & p_{11} & 0 & 0 & 0 \\ 0 & 0 & 0 & p_{44} & 0 & 0 \\ 0 & 0 & 0 & 0 & p_{44} & 0 \\ 0 & 0 & 0 & 0 & 0 & p_{44} \end{pmatrix} \tag{9}$$

with $p_{11} = -0.101$, $p_{12} = 0.0094$. From equations (7), (8), and (9), the refractive index change in x and y directions in a cubic crystal structure can be expressed as:

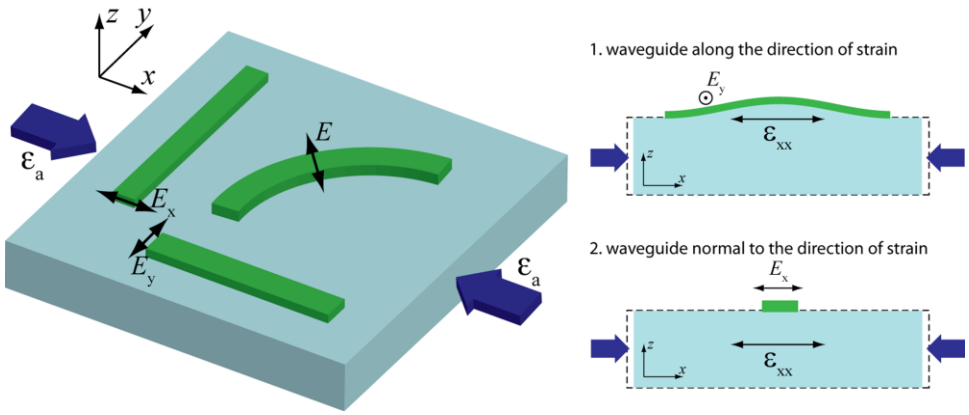

Figure S2 Single-mode waveguide under uniaxial applied strain.

$$\Delta(\frac{1}{n^2})_x = (p_{11} - 2\upsilon p_{12})\varepsilon_{xx} \tag{10}$$

$$\Delta(\frac{1}{n^2})_y = [p_{12} - (p_{11} + p_{12})\upsilon]\varepsilon_{xx} \tag{11}$$

or:

$$\Delta n_x = \frac{n^3}{2}(2\upsilon p_{12} - p_{11})\varepsilon_{xx} \tag{12}$$

$$\Delta n_y = \frac{n^3}{2}[(p_{11} + p_{12})\upsilon - p_{12}]\varepsilon_{xx} \tag{13}$$

In our system, the silicon waveguides are designed to support only the fundamental TE mode which has electric field component transverse to the waveguide direction and in the plane of the film. So the induced photo-elastic effect depends on the orientation of the waveguide with respect to the direction of applied strain as depicted in Figure S2. If the waveguide is along the direction of applied strain, i.e. the *x*-axis in Figure S2, then the non-zero electric field component of the TE mode is along the *y*-axis and only Δn_y as given by equation (13) needs to be considered in the analysis and leads to a proportional change in the waveguide mode index

$$\Delta n_{eff}^{y} = \eta \Delta n_y \tag{14}$$

The coefficient η in our waveguide design (500 nm wide, 220 nm thick) is numerically evaluated to be 1.15 for the fundamental TE mode with mode index of $n_{eff} = 2.3$.

When the waveguide is normal to the direction of applied compression, because the width of the waveguide (0.5 μm) is much smaller than the presumed buckling period

λ (37.3 μm when -3% strain is applied), the waveguide will not buckle in its transverse direction with the substrate. Thus, the induced strain and its photo-elastic effect are negligible. However, to fully understand the photo-elastic effect in a curved waveguide on a compressed substrate, more complicated modeling of the buckling effect and the resultant strain field distribution in the waveguide is needed which will be developed but is beyond the scope of the current paper.

c) Mach-Zehnder interferometer under uniaxial strain

The design of the MZI is illustrated in Figure S3. The two arms are largely symmetric except for two straight waveguide sections of length $L/2$ along the x-axis. So the geometric length difference is $\Delta L = L = 60\ \mu$m. When the substrate is compressed along the x-axis, we only need to consider the photo-elastic effect in these two sections of waveguide. The phase changes in other parts (the bends and the horizontal sections) of the interferometer are balanced in the two arms. Thus, the total phase difference between the two arms when a compressive strain is applied along the x-axis can be written as

$$\Delta\phi = \frac{2\pi}{\lambda}(n_{\text{eff}} + \Delta n_{\text{eff}}^{\text{y}}) \cdot \Delta L \tag{15}$$

The part of mechanically induced phase shift in (15) is:

$$\delta\phi(\varepsilon_{\text{a}}) = \frac{2\pi\,\Delta L}{\lambda}\Delta n_{\text{eff}}^{\text{y}} = \frac{2\pi\,\Delta L}{\lambda}\eta\ \Delta n_{\text{y}}(\varepsilon_{\text{a}}) \tag{16}$$

and the dependence of Δn_{y} on applied strain is given by equation (6) and (13).

The power transmission of the MZI can be written as:

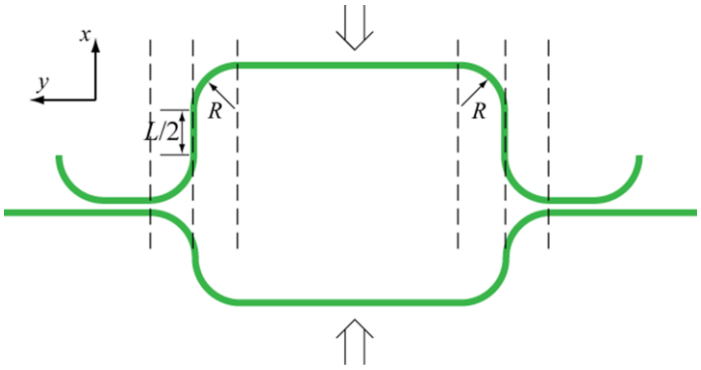

Figure S3 Geometry of Mach-Zehnder interferometer device used in the experiment.

$$T(\varepsilon_a) = \frac{1}{2}\left[1+\cos(\Delta\phi)\right] = \frac{1}{2}+\frac{1}{2}\cos\left\{\frac{2\pi\,\Delta L}{\lambda}\left[n_{\text{eff}}+\Delta n_{\text{eff}}^{y}(\varepsilon_a)\right]\right\} \quad (17)$$

and the wavelength of the fringe peak of order N is:

$$\lambda_N = \frac{1}{N}(n_{\text{eff}}+\Delta n_{\text{eff}}^{y})\cdot\Delta L \quad (18)$$

The experimental results in Figure S3 of the main text can be fitted with the above theoretical model. The fitting uses only one free parameter, which is a proportional coefficient between the nominal strain ε_n read from the mechanical stage's micrometer and the actual applied strain ε_a on the device as: $\varepsilon_a = k\varepsilon_n$. The result gives a value of 0.7 for the parameter k, which can be considered reasonable, given the non-ideal contact and friction between the stage and the sample. Thus the observed mechanical tuning of MZI device can be convincingly explained by photo-elastic effect induced by mechanical compression.

d) Micro-ring resonator under applied strain

The micro-ring resonator shows very different behavior from the MZI when it is tuned. When the substrate is compressed, the resonance wavelengths only shift slightly but the measured quality factor Q and the extinction ratio (ER) changes rapidly with the applied strain. These suggest that the photo-elastic effect in the micro-ring is weak due to relaxed strain in the structure of a closed loop or averaged out due to the symmetry of a closed

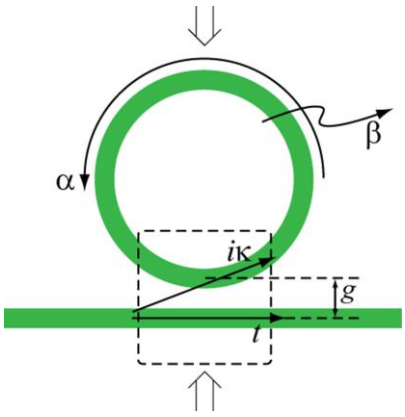

Figure S4 Geometry of the ring resonator device under mechanical tuning.

ring, whereas the coupling efficiency between the bus waveguide and the micro-ring can be changed mechanically. To fully understand the photo-elastic effect in a ring, detailed mechanics modeling of the buckling effect and the resultant strain field distribution in the waveguide is needed. Nevertheless, the latter effect can be modeled using the standard theory of waveguide coupled optical resonators[7]. As shown in Figure S4, t and $i\kappa$ denote the field transmission and coupling coefficients in the waveguide and the micro-ring coupled region (region inside the dashed box). Both t and κ are purely real and related to each other by

$$t^2 + \kappa^2 = 1 \tag{19}$$

α and β are the round trip field transmission and loss coefficients in the ring and thus they are related by

$$\alpha^2 + \beta^2 = 1 \tag{20}$$

from energy conservation. With these parameters, the waveguide loaded Q factor and on resonance intensity transmission can be expressed as

$$Q = \frac{2\pi^2 n_{\text{eff}} R}{\lambda} \frac{\sqrt{\alpha t}}{1-\alpha t} \tag{21}$$

$$T_0 = \left| \frac{\alpha - t}{1-\alpha t} \right|^2 \tag{22}$$

At the critical coupling condition of $\alpha = t$, $T_0 = 0$ and $Q_c \simeq Q_i / 2$ for large Q, where Q_i is the intrinsic Q value which can be expressed by letting t=1 in equation (21). From our measurement results in Fig. 4c of the main text, the critically coupled Q_c is ~15,000 so the intrinsic Q_i is ~30,000. From the above relations we can solve for the value of the coupling coefficient κ to be ~0.5 in this device before it is compressed. Approximately, κ is exponentially dependent on the coupling gap g, as can be understood from the coupled mode theory and confirmed by numerical simulation. It thus can be expressed as:

$$\kappa(g) = \kappa(g_0) e^{-(g-g_0)/d} \tag{23}$$

where d is the decay length and evaluated by numerical simulation to be 44 nm in our system. Combining equations (19)-(23), the Q factor and the extinction ratio $ER = 10\log_{10}(T_0)$ can be expressed in closed forms. With small displacement

approximation, the actually change of the coupling gap $\delta g = g - g_0$ is assumed to be proportional to the applied strain ε_a with a coefficient *b* as

$$\delta g = b\,\varepsilon_a \tag{24}$$

The above model was used to fit the experimental results in Fig. 4c and d of the main text with parameter *b* being the only free parameter. From the fitting result, it was determined that the coupling gap is increased to 112 nm from the initial size of 80 nm to reach the critical coupling condition when 3.7% strain is applied to the sample.

2. Repeatability test of the flexible devices

To test the repeatability and reversibility of mechanical tuning of the flexible devices, we have repeated the tuning process for more than fifty cycles of compressing and releasing. Figure S5 shows the results from a Mach-Zehnder interferometer (a) and a micro-ring resonator (b). For the MZI device, the output interference fringes shift when the sample is compressed. Figure S5a shows the transmission measured at 1570 nm and spectral shift of the fringes of a MZI device when the sample is repeatedly compressed and released in steps of 50 μm for ten times. After each cycle, the transmission recovers to within 1.8% (standard deviation, the same below) of the original value and the fringe peak wavelengths return to the original value within 0.4% of the free-spectral range (FSR). In the intermediate tuning step, the variations of transmission and fringe peak wavelengths are within 9.6% and 1.1% FSR, respectively. This large variation of measured transmission is due to the misalignment between the input/output tapered fibers and the sample when it is deformed. This issue of misalignment can be alleviated if the fibers are permanently attached to the sample, using optical epoxy for example.

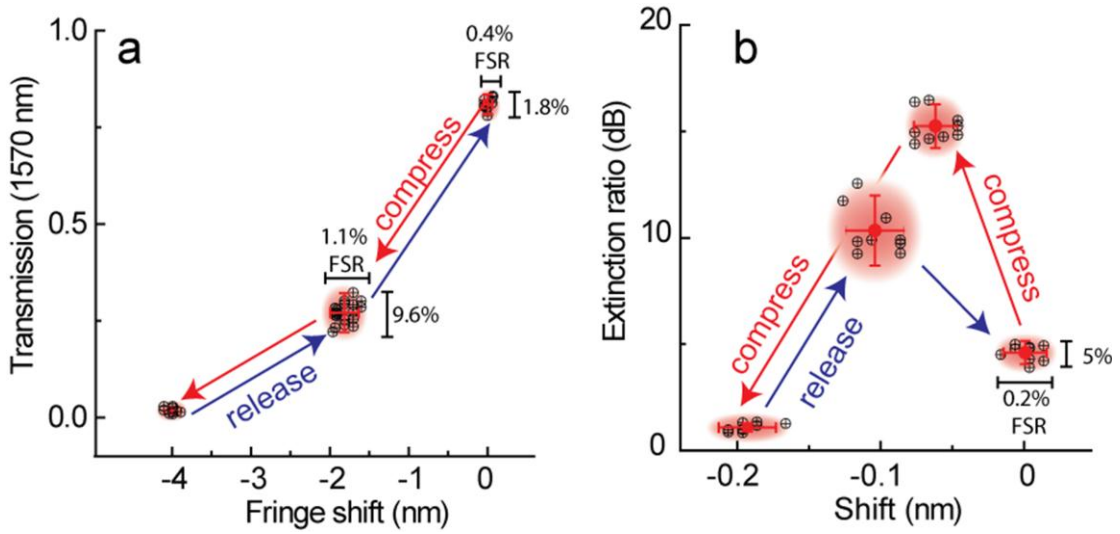

Figure S5 Geometry of Mach-Zehnder interferometer device used in the experiment.

For the micro-ring resonator, mechanically tuning changes its extinction ratio and quality factor dramatically but only slightly affect the resonance wavelengths. Figure S5b shows the result of repeatability test in which the extinction ratio and the shift of resonance wavelengths are measured in repeated tuning cycles of compression and releasing in steps of 400 μm. Like the MZI, after every cycle, the device optical properties recover to the original value within 5% for extinction ratio and 0.2% of FSR for resonance wavelengths, indicating excellent reversibility of the device. However, in the intermediate steps of tuning, large variations of ER and resonance wavelengths were observed along with a hysteretic effect between compressing and releasing. It suggests that the friction between the sample and the mechanical stage is high and the manual control of the stage displacement is imprecise. These can be solved by using an integrated actuator for mechanical tuning or a more properly designed mechanical system to avoid the friction induced hysteresis. Nevertheless, the demonstrations above show that the flexible photonic devices have very good repeatability and reversibility properties. They thus are promising to be applied in reconfigurable and adaptive optical systems.

3. Yield of the transfer process

By carefully controlling the conditions of critical processes in the transfer procedure, we can routinely achieve a device yield above 90%. For example, to ensure a calibrated and consistent etch rate in the BOX undercut etching step, temperature of the buffered oxide

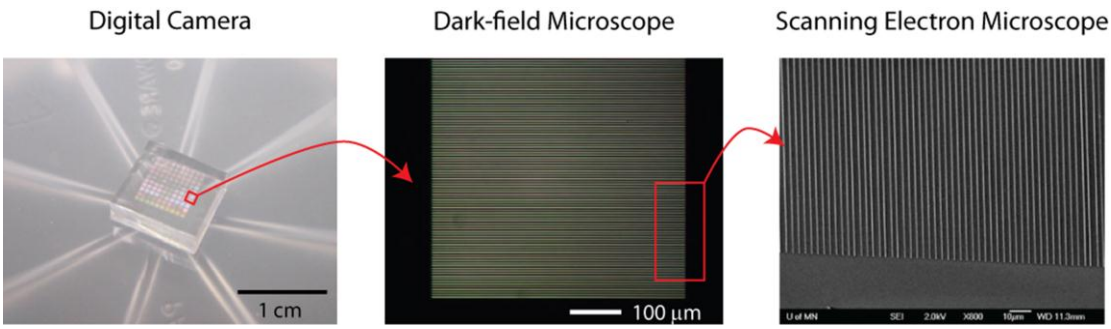

Figure S6 Images of a dense array of waveguides transferred on to a PDMS substrate, showing a high yield of the transfer process.

etchant (BOE) solution was maintained at zero degree Celsius by immersing the container in an ice-water bath. During the bonding step, the devices were placed in a heated vacuum desiccator for an hour to remove water moisture at the bonding interface. Figure S6 shows images of a large array of silicon waveguides after being transferred on to a PDMS substrate with a very high yield and negligible displacement of the waveguide from their positions on the original substrate.

Reference

1 Bowden, N., Brittain, S., Evans, A. G., Hutchinson, J. W. & Whitesides, G. M. Spontaneous formation of ordered structures in thin films of metals supported on an elastomeric polymer. *Nature* **393**, 146-149 (1998).

2 Huang, Z. Y., Hong, W. & Suo, Z. Nonlinear analyses of wrinkles in a film bonded to a compliant substrate. *Journal of the Mechanics and Physics of Solids* **53**, 2101-2118 (2005).

3 Chen, X. & Hutchinson, J. W. Herringbone buckling patterns of compressed thin films on compliant substrates. *J Appl Mech-T Asme* **71**, 597-603 (2004).

4 Jiang, H. Q. *et al.* Finite deformation mechanics in buckled thin films on compliant supports. *P Natl Acad Sci USA* **104**, 15607-15612 (2007).

5 Sun, Y. G. & Rogers, J. A. Structural forms of single crystal semiconductor nanoribbons for high-performance stretchable electronics. *J Mater Chem* **17**, 832-840 (2007).

6 Yariv, A. & Yeh, P. *Optical waves in crystals : propagation and control of laser radiation*. Wiley classics library edn, (John Wiley and Sons, 2003).

7 Yariv, A. Critical coupling and its control in optical waveguide-ring resonator systems. *Photonics Technology Letters, IEEE* **14**, 483-485 (2002).